CrossMark

ORIGINAL

Investigation of flow structure and heat transfer characteristics in an array of impinging slot jets

Yucel Ozmen[1] · Gokhan Ipek[1]

Abstract In this study, an experimental and numerical study is carried out to investigate flow field and heat transfer characteristics of unconfined and confined arrays of four turbulent slot air jets issuing from the lower surface and impinging normally on the upper surface. Pressure and temperature distributions on the surfaces were obtained for the nozzle-to-plate spacing (H/W) of 1–10 and for the Reynolds numbers in the range of 5000–15,000 at the jet-to-jet centerline spacing (S/W) of 9. The effects of jet confinement, Reynolds number and nozzle-to-plate spacing on the flow structure and heat transfer were investigated. Pressure distributions are obtained experimentally and numerically, while heat transfer distributions are computed numerically. It is observed that the surface pressure distributions on both impingement and confinement plates are independent from the Reynolds number, while they have been largely affected from the nozzle-to-plate spacing. Jet confinement causes a considerable difference at the flow field especially for small nozzle-to-plate spacings. Subatmospheric regions are not observed for unconfined jet. However three different types of subatmospheric pressure regions occur on both impingement and confinement plates for confined jet. Nusselt distributions on the impingement plate for both unconfined and confined jet configurations depend on the Reynolds number and nozzle-to-plate spacing. It is concluded that there is a strong correlation between subatmospheric regions and secondary peaks in Nusselt distributions. The numerical results obtained using the Realizable k-ε turbulence model is in good accordance with the experimental results for moderate values of nozzle-to-plate spacings.

List of symbols

C_p	Pressure coefficient ($\Delta P/(\rho U_o^2/2)$)
C	Specific heat at constant pressure (J/ kg K)
$C_1, C_\mu, C_2, C_{1\varepsilon}, C_{3\varepsilon}$	Constants in the Realizable k-ε turbulence model
E	Total energy (J)
G_b	Generation of turbulent kinetic energy due to buoyancy
G_k	Production of turbulent kinetic energy due to velocity gradients
h	Convective heat transfer coefficient (W/m^{2}K)
H	Nozzle-to-plate spacing (m)
k	Turbulent kinetic energy (m^2/s^2)
k_a	Thermal conductivity of air (W/m K)
L	Length of slot nozzle (m)
Nu	Nusselt number (h W/k$_a$)
ΔP	Difference between the surface pressure and the atmospheric pressure (N/m^2)
p	Pressure (N/m^2)
q	Convective heat flux (W/m^2)
Re	Slot nozzle Reynolds number ($U_o W/\upsilon$)
S	Jet-to-jet centerline spacing (m)
S_k, S_ε	Source terms
T	Temperature (K)
T_w	Impingement wall temperature (K)
T_j	Jet exit temperature (K)
V_o	Nozzle exit velocity (m/s)

✉ Yucel Ozmen
   yozmen@ktu.edu.tr

   Gokhan Ipek
   ipekgokhan@yahoo.com.tr

[1] Department of Mechanical Engineering, Karadeniz Technical University, 61080 Trabzon, Turkey

u, v, w	Velocity components in x, y and z directions (m/s)
u_τ	Friction velocity (m/s)
W	Slot nozzle width (m)
x	Displacement on the plates along direction of slot width (m)
y	Displacement along direction of jet axes (m)
z	Displacement on the plates along direction of slot length (m)
y^+	Dimensionless distance ($y^+ = yu_\tau/\upsilon$)
υ	Kinematic viscosity (m²/s)
ρ	Density of air (kg/m³)
ε	Turbulent dissipation rate (m²/s³)
$(\tau_{ij})_{eff}$	Deviatoric stress tensor
μ_{eff}	Effective viscosity (kg/ms)
μ	Laminar viscosity (kg/ms)
μ_t	Turbulent viscosity
δ_{ij}	Kronecher delta function
$\sigma_k, \sigma_\varepsilon$	Turbulent Prandtl numbers
Y_M	Fluctuation rates related to the overall dissipated turbulent thermal energy

1 Introduction

Impinging fluid jets are widely used in many industrial applications because of their highly attractive local heat and mass transfer characteristics. The application of jet impingement include tempering and shaping of glass, drying of paper and textiles, annealing of metal sheets and cooling of turbine blades and electronic components. Over the past 30 years, experimental and numerical investigations of flow and heat transfer characteristics under single and multiple impinging jets became a very dynamic research area. Although the single impinging jets yield very high heat transfer coefficients in the stagnation zone, the cooling performance drops rapidly away from the impinging zone. For this reason, impinging jets are often used as array in many applications. In such case, the interaction between the jets in the array plays an important role in the cooling performance. Numerous studies have been reported in the literature on the flow, heat and mass transfer distributions of impinging jets. Most of the previous studies on this are concerned with heat transfer rates of unconfined and confined single and multiple jets impinging on a plate. However, very few of them are concerned about flow structure of the multiple impinging jets, especially about slot jets despite their popularity in application. Impinging jets on the flat plates are frequently used in industrial practice requiring the subatmospheric region. Confined impinging jets produce recirculation zones in the flow field.

This zones cause subatmospheric pressure regions on the impingement and confinement surfaces at low nozzle-to-plate spacings. Particularly, it is investigated the presence of these regions to find a correlation between the subatmospheric regions and the peaks in the Nusselt distributions on the impingement surface.

Martin [1] and Polat et al. [2] reviewed the heat transfer characteristics of multiple impinging air jets without cross-flow. Bernhard and Sebastian [3] reviewed the flow and heat transfer characteristics of multiple impinging jets and compared with single impinging jets. Huber and Viskanta [4] have examined the influence of spent air located between the jets on local heat transfer coefficient for a confined impinging array of air jets. Saad et al. [5] compared the turbulence, mean flow and heat transfer characteristics of an array of confined impinging slot jet with those of a single jet. The fluid flow and heat transfer characteristics of multiple impinging slot jets with an inclined confinement surface was studied by Yang and Shyu [6]. Their results show that the maximum local Nusselt number and maximum pressure on the impingement surface move downstream while the inclination angle was increasing. Koopman [7] obtained high heat transfer coefficients for multiple jets in the stagnation region and at the second stagnation point (the midpoint between the two neighboring jets). An experimental study was carried out by Kwok et al. [8] to investigate the shape and the heat transfer characteristics of an array of three laminar pre-mixed butane/air slot flame jets impinging upwards normally on a horizontal water-cooled flat plate. It is seen from the results that the resultant heat flux distribution of the central jet of a multiple slot jets system is higher than that of a single slot jet when the jet-to-jet spacing is small. Besides, the area-averaged heat flux of the multiple slot flame jets is higher than that of the multiple round flame jets arranged at the same geometric configuration. Ozmen [9] carried out an experimental study to investigate flow characteristics of confined twin jets issuing from the lower surface and impinging normally on the upper surface for Reynolds numbers up to 50,000 at the various nozzle-to plate spacing and jet-to-jet spacing. It is concluded that there is relation between the subatmospheric regions and peaks in heat transfer coefficients for low spacing in the impinging jets. Koopman and Sparrow [10] studied a row of impinging air jets and concluded that a higher local heat transfer coefficient was obtained in the middle between adjacent jets owing to the collision of their spreading flows. Chander and Ray [11] conducted an experimental study for three interacting methane/air flame jets (arranged in a triangular configuration) impinging normally on a flat surface. Pan and Webb [12] studied local heat transfer details of the circular jet array impingement. San et al. [13] has identified the effect of jet-to-jet spacing(s) on turbulent heat transfer for an array of five

round jets for different Reynolds numbers. Rady and Arquis [14] investigated heat transfer and fluid flow characteristics during multiple laminar slot jet impingement cooling a flat plate with symmetrical exhaust ports in the confinement surface. Prasad et al. [15] investigated fluid flow and heat transfer characteristics of turbulent multiple circular jets impinging on a flat plate numerically and experimentally. They founded that primary pressure peaks are observed at the stagnation point and the secondary peaks are noticed at the interaction points of wall jets and a strong correlation between Nusselt number and the pressure distribution is noticed.

Fernandez et al. [16] investigated numerically the flow field of a turbulent twin plane jet impinging normally onto a flat surface by using Standard k-ε, Realizable k-ε and Standard k-ω turbulence models and concluded that none of the turbulence models correctly predicts the flow in the impact region. The flow and heat transfer characteristics of impinging laminar square twin jets have been numerically investigated by Aldabbagh and Sezai [17]. The calculated results show that the flow structure of square twin jets impinging on a heated plate is strongly affected by the jet-to-plate distance. A two dimensional numerical model was used by Chuang et al. [18] to determine the flow characteristics associated with an unsteady, compressible impinging twin slot jet between two plates. The results show that several recirculating zones are distributed around the flow field. In addition, a fountain upwash flow occurs between the nozzles, and two low-pressure recirculating zones are induced by the interaction between the nozzle mainstream and the fountain upwash flow. The three dimensional turbulent impinging square twin-jets with no cross flow is analyzed by Chuang and Nieh [19] using PHOENICS code. The calculated results show that the size and location of the recirculating zones around the jets are different from the two dimensional flow fields due to the effect of stretching in the transverse direction. Seyedein et al. [20] used the numerical method to simulate the two dimensional turbulent flow and heat transfer from confined multiple impinging slot jets. Xing et al. [21] conducted a combined experimental and numerical investigation of the heat transfer characteristics within an array of impinging jets. Kumar and Prasad [22] investigated flow and heat transfer of multiple circular jets impinging on a flat surface with effusion. Mikhail et al. [23] numerically predicted the Nusselt number distribution for a row of unconfined laminar slot jets impinging on an isothermal flat plate. It was shown that Nusselt number decreased from the stagnation maximum to a minimum value and then increased again, reaching a secondary peak at the line of symmetry. These phenomena were explained by the appearance of the separated and recirculating flow formed between adjacent slot jets. Cziesla et al. [24] numerically obtained Nusselt

number distributions for impinging jet array of slot nozzles (rectangular jets) by using large-eddy simulation (LES) and the direct numerical simulation (DNS). Coussirat et al. [25] performed a numerical analysis of the flow behavior in industrial cooling systems based on arrays of impinging jets using several eddy viscosity models to determine their modeling capabilities. The results obtained show that the predicted thermal field depends strongly on the combination of near-wall treatment and selected turbulence model. Garimella and Schoeder [26] have studied the local heat transfer distributions for three different configurations of in-line jet arrays compared with a single jet. They noticed that the central jet in the nine jet array generated a higher heat transfer coefficient at the stagnation point in comparison with the single jet at the same Reynolds number.

Jets array impingement on the target plate and interaction between pairs of adjacent jets are very complicated phenomena. Pressure distributions of the multiple jets are rather different from those of the single jet due to the existence of jet-to-jet interactions which can't be identified from the single jet system. Pressure distributions on the impingement plate in multiple jets greatly affect local heat transfer. The present study is performed to investigation pressure and temperature distribution of a row of four turbulent impinging slot air jets experimentally and numerically. The effect of jet flow parameters, such as nozzle-to-plate spacing and confined and unconfined jet configurations, and resulting flow parameters including surface pressure distributions on the impingement and confinement plates and Nusselt distributions on the impingement plate were examined for Reynolds numbers of 5000, 10,000 and 15,000, nozzle-to-plate spacings of 1, 2, 3, 4, 6, 8 and 10 and jet-to-jet centerline spacing of 9. The main aim of the study is to investigate the effect of the interaction between the jets on the flow structure and heat transfer and to investigate the effect of subatmospheric regions on the local heat transfer for both confined and unconfined jet configurations. The second aim is to investigate the effect of varying nozzle-to-plate spacing and Reynolds number on the pressure and temperature distribution. The third aim is to study the performance of used turbulence model in predicting three dimensional turbulent flow and heat transfer from impinging slot jet array.

2 Experimental study

The impingement slot jet array system of the present study is shown schematically in Fig. 1a, b. The air exiting from slot nozzles impinges on a flat plate. The impingement plate was mounted perpendicularly to the jets axes at various spacings according to the confinement plate. The air is supplied by a centrifugal fan mounted below the base plate via a plenum
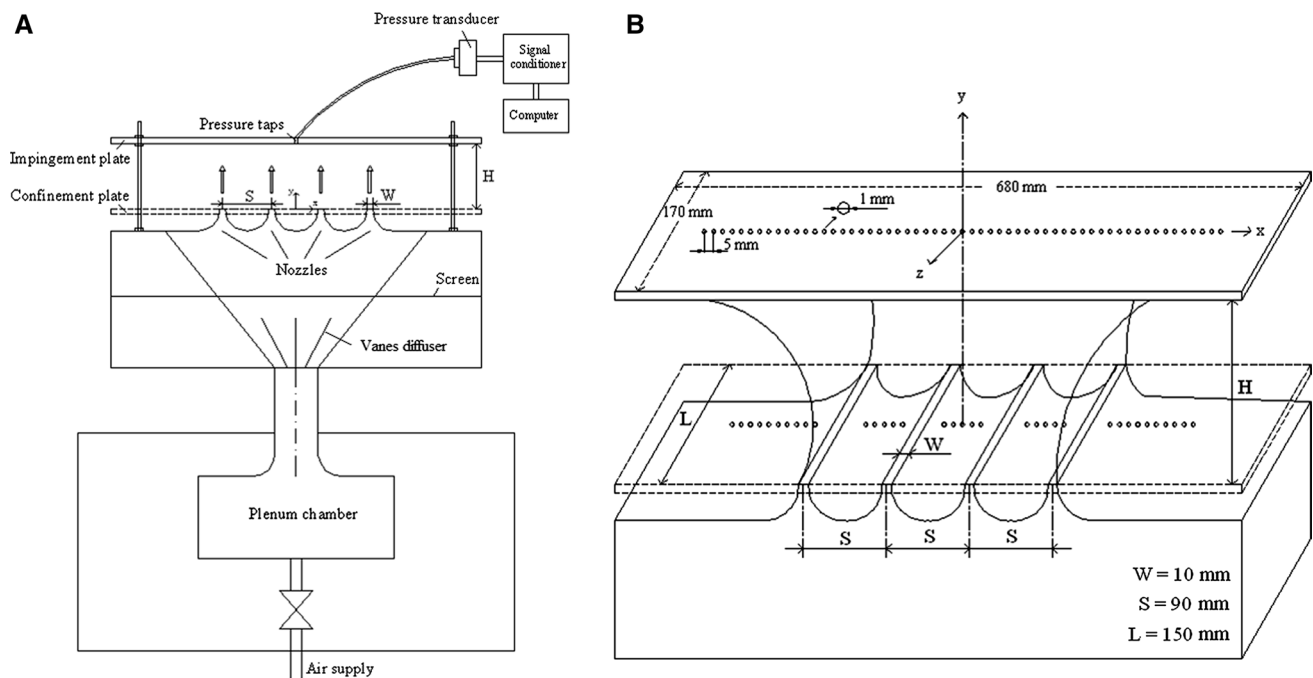
Fig. 1 Experimental setup. **a** Schematic and **b** impingement slot jet system

chamber containing a gauze screen and vanes diffuser to ensure a uniform flow towards to the nozzles. The air flow is regulated by a valve (Fig. 1a). Four identical slot nozzles with the dimensions of W = 10 mm width and L = 150 mm length is used in the jet array system. S = 90 mm represents the jet-to-jet centerline spacing. The impingement and confinement plates made of plexiglas were 680 mm length, 170 mm weight and 10 mm thickness. The confinement plate which is removed in unconfined jet studies was placed at the nozzles exits plane parallel to the impingement plate. The air jets impinge vertically onto the impingement plate at distance H from the nozzles and enter ambient air. The exit velocities of jet array were determined by means of Prandtl tube. Impingement surface pressures were measured with 90 pressure taps spaced 5 mm apart placed along the mid span centerline of the impingement plate in the x direction. For the pressure measurements on confinement plate, 48 pressure taps spaced 5 mm apart are located in streamwise direction (x direction) along the mid span centerline of confinement plate. All pressure taps used for surface pressure measurements on both impingement and confinement plates have 0.8 mm inner diameter (Fig. 1b).

Surface pressure measurements were carried out using a Setra 239 pressure transducer. Pressure taps on the impingement and confinement plates were connected to a scanivalve by 600 mm long pieces with 1 mm internal diameter PVC tubes. The data were collected at a sampling frequency of 1000 Hz for 8 s at each point. The signal from

the transducer were low-pass filtered at 300 Hz and were digitally sampled. The pressure measurements were made for the nozzle-to-plate spacing of 1–10, the Reynolds numbers ranging from 5000 to 15,000 and jet-to-jet centerline spacing of 9 in both confined and unconfined jet configurations. The Reynolds number depends on the slot nozzle width, W and the nozzle exit velocity V_o, which is measured with the pitot tube. The jet velocities at the nozzles exit were 7.5, 15 and 22.5 m/s. The pressure coefficient, C_p, is defined as $C_p = (\Delta P)/0.5 \; \rho V_o^2$. ΔP represents the difference between the local pressure on the impingement and confinement plates and the atmospheric pressure and $(0.5 \; \rho V_o^2)$ is the dynamic pressure, where ρ is the density of air, V_o is the exit velocity of the jets. Nozzle-to-plate spacing, H and distance along the mid span centerline of plates, x has been normalized by the slot nozzle width, W. Uncertainty in pressure measurements at the impingement and confinement plates was about ±2.4 %. The experimental results were reproducible within these uncertainty ranges.

3 Numerical study

3.1 Mathematical model

In the present study, it is assumed that the air flow is turbulent, steady-state and Newtonian with temperature-dependent fluid properties. A numerical solution of the mean flow

Fig. 2 Schematic of the jet array configuration and computational domain
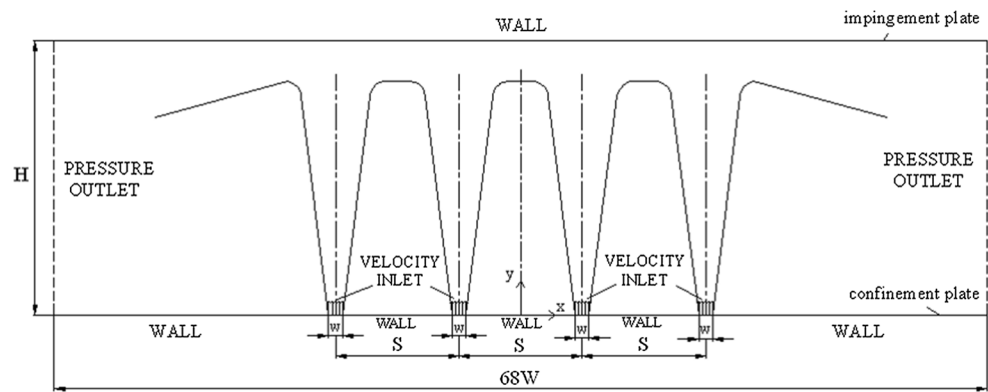
and thermal fields requires resolving the Reynolds averaged Navier–Stokes equations and energy equation. These equations for three-dimensional, incompressible and continuity flow in Cartesian tensor form can be written as given below, mass continuity:

$$\frac{\partial}{\partial x_i}(\rho u_i) = 0 \tag{1}$$

momentum:

$$\frac{\partial}{\partial x_j}(\rho u_i u_j) = -\frac{\partial P}{\partial x_i} + \frac{\partial}{\partial x_j}\left[\mu\left(\frac{\partial u_i}{\partial x_j} + \frac{\partial u_j}{\partial x_i} - \frac{2}{3}\delta_{ij}\frac{\partial u_i}{\partial x_j}\right)\right]$$
$$+ \frac{\partial}{\partial x_j}\left(-\overline{\rho u_i' u_j'}\right) \tag{2}$$

where, the term $\left(-\overline{\rho u_i' u_j'}\right)$ is the Reynolds stress, defined as

$$-\overline{\rho u_i' u_j'} = \mu_t\left(\frac{\partial u_i}{\partial x_j} + \frac{\partial u_j}{\partial x_i}\right) - \frac{2}{3}\left(\rho k + \mu_t\frac{\partial u_i}{\partial x_i}\right)\delta_{ij} \tag{3}$$

energy:

$$\frac{\partial}{\partial x_i}[u_i(\rho E + P)] = \frac{\partial}{\partial x_j}\left[\left(k + \frac{C\mu_t}{\Pr_t}\right)\frac{\partial T}{\partial x_j} + u_i(\tau_{ij})_{eff}\right] \tag{4}$$

where E is the total energy, $E = CT - \frac{P}{\rho} + \frac{u^2}{2}$ and $(\tau_{ij})_{eff}$ is the deviatoric stress tensor, defined as

$$(\tau_{ij})_{eff} = \mu_{eff}\left(\frac{\partial u_j}{\partial x_i} + \frac{\partial u_i}{\partial x_j}\right) - \frac{2}{3}\mu_{eff}\frac{\partial u_i}{\partial x_j}\delta_{ij} \tag{5}$$

Numerical solutions are performed by using Realizable k-ε turbulence model because of capturing the near-wall turbulence effects more accurately. This model consists of two transport equations which solve the turbulent kinetic energy (k) and turbulent dissipation rate (ε). The transport equations are as follows:

$$\frac{\partial}{\partial x_i}(\rho k u_j) = \frac{\partial}{\partial x_i}\left[\left(\mu + \frac{\mu_t}{\sigma_k}\right)\frac{\partial k}{\partial x_j}\right] + G_k + G_b$$
$$- \rho\varepsilon - Y_M + S_k \tag{6}$$

$$\frac{\partial}{\partial x_j}(\rho\varepsilon u_j) = \frac{\partial}{\partial x_j}\left[\left(\mu + \frac{\mu_t}{\sigma_\varepsilon}\right)\frac{\partial\varepsilon}{\partial x_j}\right] + \rho C_1 S_\varepsilon$$
$$- \rho C_2\frac{\varepsilon^2}{k + \sqrt{\nu\varepsilon}} + C_{1\varepsilon}\frac{\varepsilon}{k}C_{3\varepsilon}G_b + S_\varepsilon \tag{7}$$

where G_k is the production of turbulent kinetic energy due to the mean velocity gradients, G_b represents the generation of the turbulent kinetic energy due to buoyancy while Y_M is referred to the fluctuation rates related to the overall dissipated turbulent thermal energy. σ_k and σ_ε represent the turbulent Prandtl numbers based on k and ε, respectively; while S_k and S_ε are further generation terms. The turbulent viscosity is defined by

$$\mu_t = \rho C_\mu\frac{k^2}{\varepsilon} \tag{8}$$

The model constants for the Realizable k-ε model are given by:
$$C_{1\varepsilon} = 1.44, \quad C_2 = 1.9, \quad \sigma_k = 1.0 \quad \text{and} \quad \sigma_\varepsilon = 1.2.$$
C_μ is no longer a constant in this model.

3.2 Flow field and boundary conditions

A schematic of the slot jet array configuration and computational domain is shown in Fig. 2 where the flow field, the main dimensions and the prescribed boundary conditions are specified. Four strong main jets are injected through upward from the slot nozzles of width W = 10 mm with a uniform velocity V_o and induced the surrounding flow to enter the flow field. The flow direction of the fluid is spread into the surrounding when the array of air jets impinges perpendicularly on a plate at a distance H from the nozzles. S represents the jet-to-jet centerline spacing. The length of computational domain in the x-direction is approximately 68 W. The following boundary conditions were used: the impingement plate was specified as an isothermal wall and constant temperature condition are used as $T_w = 333$ K, jet exit temperature was taken as constant temperature of

Fig. 3 Grid arrangement in the computational domain. **a** 3D and **b** x–z plane
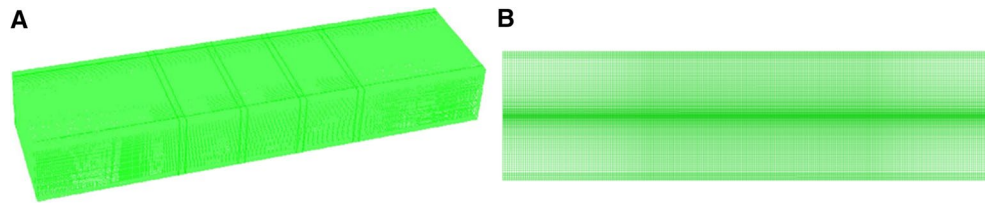
$T_j = 293$ K which was equal to confinement plate temperature and no-slip condition were specified on every wall; the mean velocity and turbulence profiles measured at the nozzles exit were used as velocity inlet conditions of computational domain and pressure outlet boundary conditions were assumed at outlet planes.

3.3 Numerical solution procedure

The governing equations were solved using the FLUENT 6.3.26 software, by finite volume discretization, using a segregated solver with an implicit formulation. For the 3D simulations the diffusion and convective terms in the equations were approximated by second order upwind scheme. The discretized equations for the pressure–velocity coupling were solved by using the SIMPLEC algorithm on staggered grids. SIMPLEC procedure uses modified equation for face flux correction. The use of modified correction equation accelerates convergence. Pressure was solved using standard discretization scheme. A second order discretization method was used for the other variables (momentum, turbulent kinetic energy, turbulence dissipation rate and energy equation). Second order discretization scheme presents higher-order accuracy especially for complex flows involving separation. Enhancement wall treatment was used as wall function to obtain reasonably accurate predictions near the wall. Enhanced wall treatment is a near-wall modeling method that combines a two-layer model with enhanced wall functions. The two-layer approach is an integral part of the enhanced wall treatment and is used to specify the turbulent viscosity in the near-wall cells. In this approach, the whole domain is subdivided into a viscosity-affected region and a fully-turbulent region. Thus, more accurate results are obtained near the wall. The convergence criterion for the residuals was set to 1×10^{-5} for all dependent variables. Figure 3 shows the grid generated for the numerical simulation. Finer grids are used adjacent to mid-span of impingement surface. To ensure the attainment of grid-independent results, sensitivities of both grid numbers and grid distributions were tested for each case. The mesh used is refined for each value of H/W until negligible differences are obtained. Finer computational grids were set near the wall and y^+ was less than 2.5. Refined grid density of 1,000,000 in the whole computational domain is sufficient.

4 Results and discussion

Experimental and numerical investigations were carried out for the nozzle-to-plate spacings (H/W) of 1–10 and the Reynolds numbers in the range of 5000–15,000 at the jet-to-jet centerline spacing (S/W) of 9 for both unconfined and confined impinging slot jets array. Experimental study was performed to obtain surface pressure distributions on the mid span centerline of impingement and confinement plates. Numerical study was conducted to compute streamlines, surface pressure and Nusselt distributions.

4.1 Flow structure

Streamlines of the predicted velocity fields on the mid-vertical xy plane at H/W = 1, 2 and 4 with Re = 10,000 are given in Figs. 4 and 5 for unconfined and confined jet
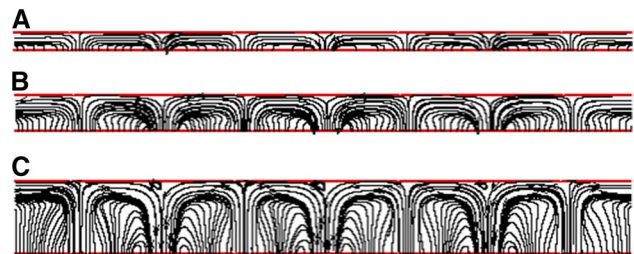

Fig. 4 Computed streamlines images on the mid vertical xy plane for unconfined jet configuration at S/W = 9 and Re = 10,000. **a** H/W = 1, **b** H/W = 2 and **c** H/W = 4

Fig. 5 Computed streamlines images on the mid vertical xy plane for confined jet configuration at S/W = 9 and Re = 10,000. **a** H/W = 1, **b** H/W = 2 and **c** H/W = 4

configurations respectively. In the array of four imping-
ing slot jets, two jets in the middle are named as central
jets and the other two jets are specified as side jets. The
configuration of two central jets surrounded by two side
jets is similar to the situation of any jets in a jet array. The
central jets experience interference from them two neigh-
boring jets and the effect can be used to characterize the
behavior of any jet in a large jet array except that at the
free end, which is affected by the neighboring jet from
one side only [8]. For unconfined jet, each of the four jets
has basically the similar shape. Air jets issuing from the
slot nozzles in the y direction veer to the x direction near
the impingement regions and form bidirectional wall jets
along the impingement plate. Two different types (of)
stagnation points occur on the impingement plate. Pri-
mary stagnation points are at the direction of nozzle axes,
secondary stagnation points are at the midpoint of neigh-
bor two jets. At the secondary stagnation points, due to
the interaction between the adjacent jets, jets change
their direction again and they discharge to the ambient
air. Downwash fountain flows occur between the jets due
to the collision of the wall jets and entrainment of ambi-
ent air. Level of the interaction is affected from H/W.
At lower nozzle-to-plate spacings, the wall jets fill the
almost whole gap in the flow filed (Fig. 4a). For confined
jet, array of slot jets after impinging on the impingement
plate spread along the wall. Between the jets, second-
ary stagnation regions form on the impingement plate by
the collision of the lower wall jets. Recirculation regions
occur at the both sides of the central jets and other neigh-
bor jets. After jets impinge on the impingement plate,
they spread along the wall. These behaviors of the cen-
tral jets suppress the motion of neighbor jets in the axial
direction and cause their orientation to the x direction
without impinging on the impingement plate. Central
jets push the side jets outwards. Air jets exiting from slot
nozzles impinge the impingement plate and form coun-
ter-rotating vortices because of confinement plate. With
increasing H/W spacing, recirculation regions occurring
at the both sides of the central jets effect the development
of other neighbor jets in the flow direction. The sizes of
the recirculation regions increase with increasing H/W
(Fig. 5). The evolution of the wall jets is illustrated in
Fig. 6a, b through a projection of the streamline images
on a horizontal plane (x–z plane) near the impingement
plate at the Re = 10,000 and H/W = 3 for unconfined
and confined jet configurations respectively. Slot jets veer
near the impingement plate and form wall jets. Except
end regions, occurring the same streamlines along the
slot length show that the flow field can be investigated as
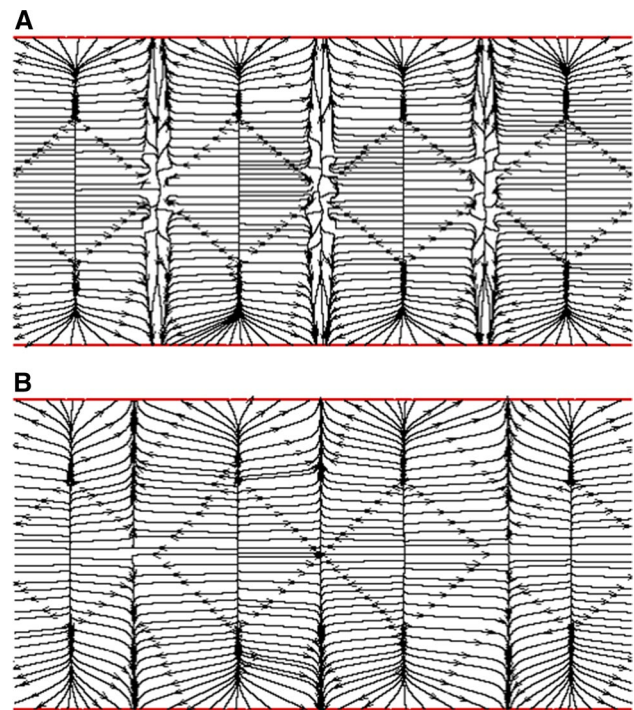2D. Similar images are obtained for confined jet with the
same parameters.

Fig. 6 Computed streamlines images on a horizontal xz plane near
impingement plate at H/W = 3 and Re = 10,000. **a** Unconfined jet
and **b** confined jet

4.2 Pressure distributions

The effect of the nozzle-to-plate spacing (H/W) to the local
surface pressure distributions on the impingement plate
for unconfined jet and on the impingement and confine-
ment plates for confined jet at Re = 10,000 are shown in
Fig. 7a–c respectively.

Figure 7a shows the pressure distributions on the
impingement plate for unconfined jet configuration for dif-
ferent H/W ratios at Re = 10,000. Four primary stagnation
points occur on the impingement plate at the direction of
jets axes while three secondary stagnation points occur at
the mid points between adjacent jets. The maximum pres-
sures occur at the stagnation points for all nozzle-to-plate
spacing studied. Local pressures at primary and secondary
stagnation points on the impingement plate have nearly the
same maximum values for the same spacing. At low noz-
zle-to-plate spacing (H/W = 1), primary stagnation pres-
sures are larger than 1 due to rapidly decreasing of axial
velocity in the deflection zone. For low nozzle-to-plate
spacings, near the stagnation points, the flow rapidly decel-
erates and therefore pressure increases significantly. This
situation is because of flow orientation originating small
distance between nozzles exit and impingement plate.
The maximum values at the stagnation points decrease

Fig. 7 Effect of the nozzle-to-plate spacing on the pressure distribution for Re = 10,000. **a** Impingement plate in unconfined jet, **b** impingement plate in confined jet and **c** confinement plate in confined jet
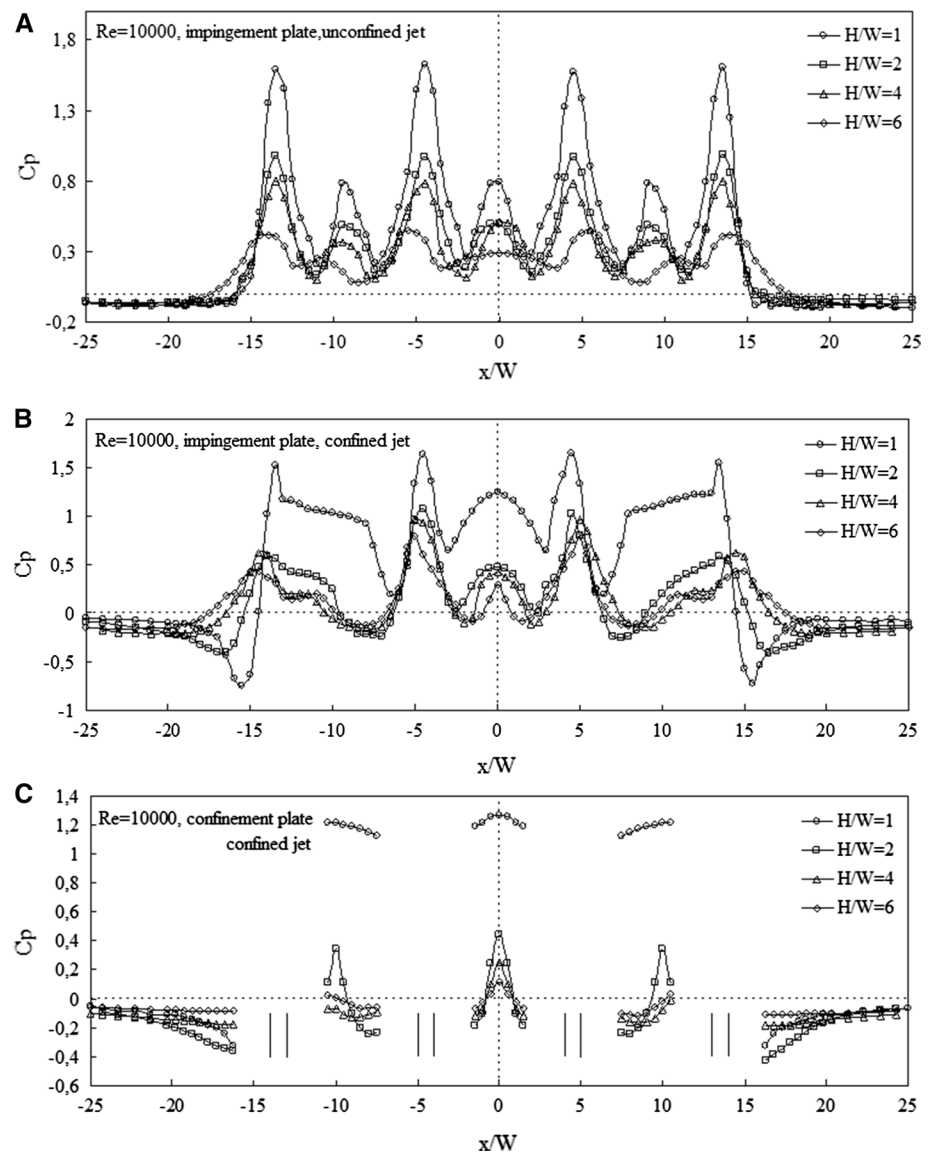
with increasing H/W spacings. Secondary pressure peaks are observed at the secondary stagnation points where neighboring wall jets collide. Pressure peaks at primary stagnation points are greater than the peak values at the secondary stagnation points. No suboatmopheric region is observed on the impingement plate for spacings studied. This situation can be explained with the fluid velocity along the impingement plate is lower with respect to the confined jets due to no flow confinement. For all the studied spacings, local pressures taking their maximum values at the primary stagnation points of side jets suddenly decrease around x/W = ±15 and beyond approach the atmospheric value to the ends of impingement plate. Figure 7b, c show the pressure distribution on impingement and confinement plates for different H/W ratios at S/W = 9 and Re = 10,000. Three types of subatmospheric region occur on the impingement and confinement

plates depending on nozzle-to-plate spacing. Primary subatmospheric regions occur on the impingement plate along the outwards of side jets for all studied spacings and they become stronger decreasing nozzle-to-plate spacing. These primary subatmospheric regions shift to outward distances with increasing nozzle-to-plate spacing due to jet spreading. Secondary subatmospheric regions occur between the side and central jets while tertiary subatmospheric regions occur between the central jets. At the H/W = 1, only primary subatmospheric regions occur on the impingement plate with the same magnitude. Secondary and tertiary subatmospheric regions are observed on the impingement plate for the spacing of H/W ≥ 2. Secondary subatmospheric regions is weaker than primary subatmospheric regions at H/W = 2. As nozzle-to-plate spacings increase, the fluid velocity decreases due to jets spreading, and thus the strength of the all subatmospheric regions decrease. For

Fig. 8 Effect of the Reynolds number on the pressure distribution for H/W = 1. **a** Impingement plate in unconfined jet, **b** impingement plate in confined jet and **c** confinement plate in confined jet
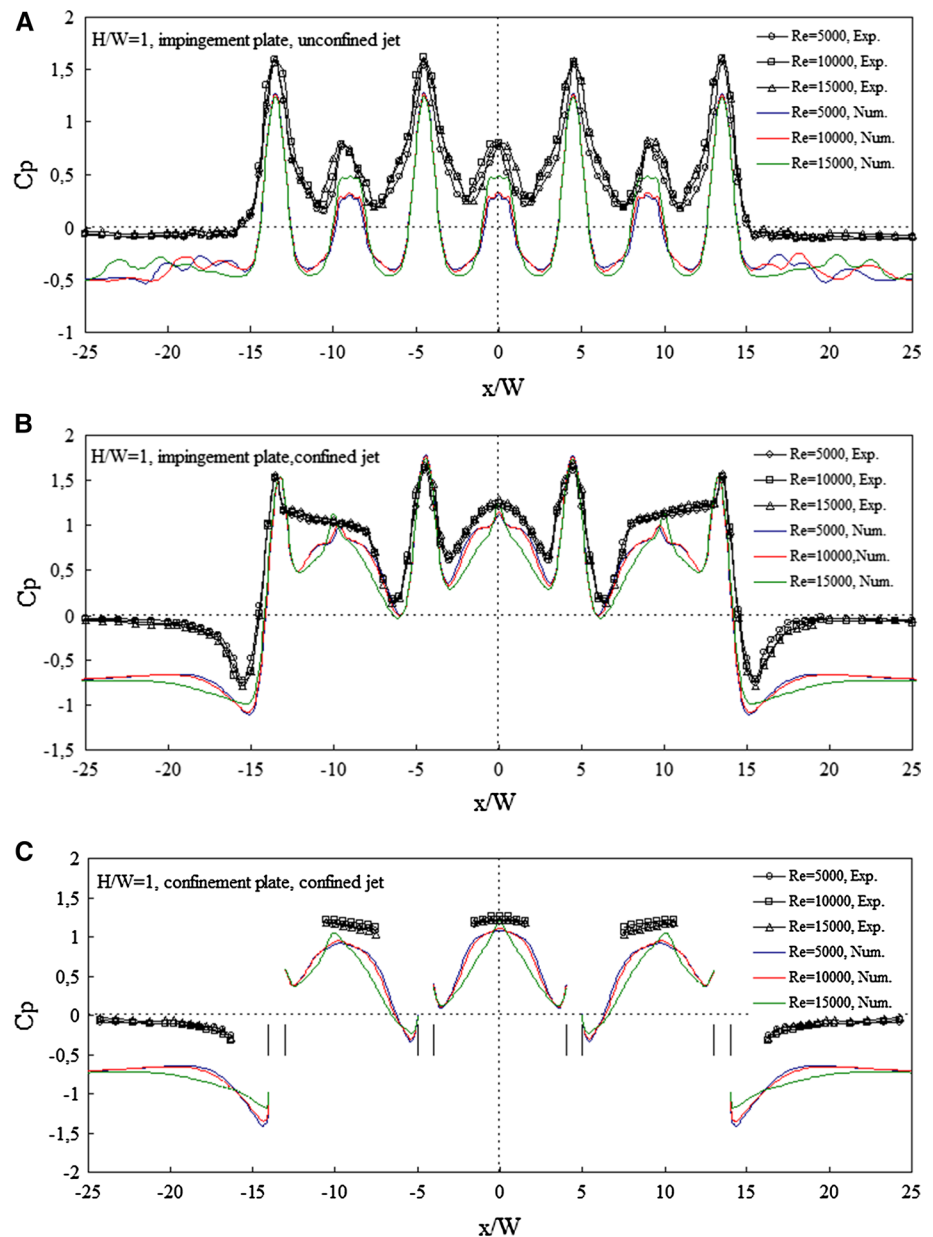
the $H/W > 2$, subatmospheric regions on the impingement plate have almost the same magnitude. There observed subatmospheric regions on the impingement plate for spacings up H/W = 8. Similar to the impingement plate, subatmospheric regions occur on the confinement plate at the both sides of the slot nozzles. Subatmospheric regions on the confinement plate become poorer at H/W = 8 and get lost at larger H/W = 10. Maximum pressures caused central jets are greater than those of originated side jets at the primary stagnation points. This situation can be explained with the orientation of central jets to side jets to form wall jets. Central jets suppress and push the side jets outwards. As H/W space increases, stagnation point pressure values decreases. On the impingement plate, there is no clear pressure peaks at the secondary stagnation points except for secondary stagnation point occurred between central jets. While local pressure takes positive values at the region between the side jet axes for H/W = 1, new subatmospheric regions occur at the region between the side jets on the impingement and confinement plates $H/W > 1$ spacings. These subatmospheric regions support presence of reverse flow regions. At all studied spacing, subatmospheric pressure regions occur on the impingement and confinement plates. With increasing H/W, local pressures on the confinement plate approach to ambient value. When the pressure distributions on the impingement plate for unconfined and confined jet configurations compare each other, it is seen that subatmospheric regions occur only for confined

Fig. 9 Effect of the Reynolds number on the pressure distribution for H/W = 2. **a** Impingement plate in unconfined jet, **b** impingement plate in confined jet and **c** confinement plate in confined jet
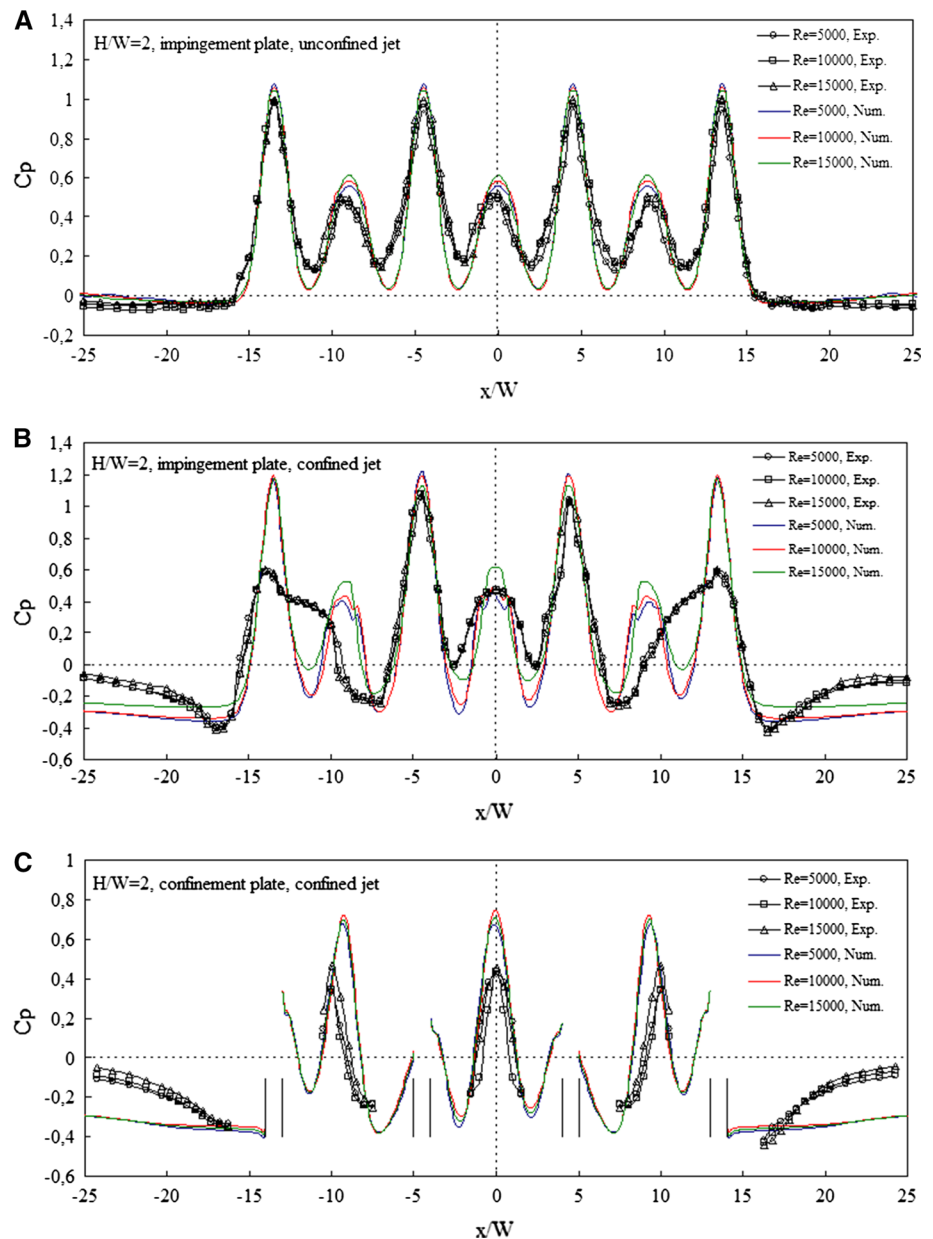

jet case. For both jet configurations, maximum pressure (pressure peaks) occur stagnation points and decrease from these points for all studied H/W. For H/W = 1, pressure peaks at the primary stagnation points for both jet configurations have almost the same magnitude. For $H/W \geq 2$, pressure peaks of central jets are greater for confined jet, while the pressure peaks of side jets are higher for unconfined jet. While low spacing, at the region between side jets axes, local pressures are greater for confined jet, for high spacings, because of forming of subatmospheric regions, local pressures take bigger values at the same region for unconfined jet. Difference between the local pressures distributions of unconfined and confined jet configurations on

the impingement plate decreases with increasing H/W and get lost at H/W = 10.

The effect of the Reynolds numbers on the local surface pressure distributions obtained experimentally and numerically for unconfined and confined jet are shown in Figs. 8, 9 and 10 for the nozzle-to-plate spacings of H/W = 1, 2 and 4, respectively. It is observed from experimental and numerical results obtained for all studied spacings, in general, that the surface pressure distributions are independent of the Reynolds number, while they depend strongly on the nozzle-to-plate spacing. Locations where pressures occur maximum are the same on the impingement plate for all studied Reynolds numbers. At the stagnation points, the

Fig. 10 Effect of the Reynolds number on the pressure distribution for H/W = 4. **a** Impingement plate in unconfined jet, **b** impingement plate in confined jet and **c** confinement plate in confined jet
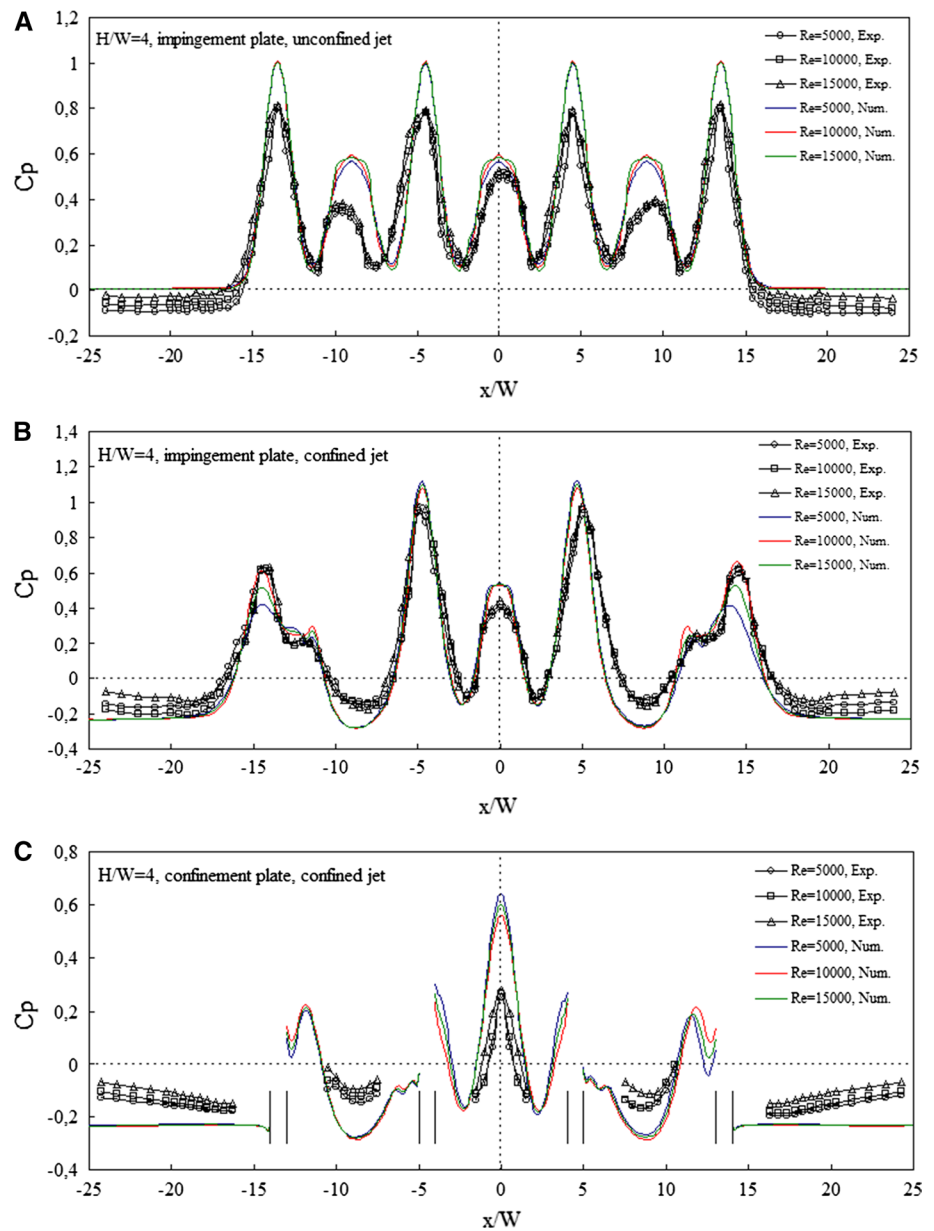
velocity is zero and the pressure is maximum, and on the other impingement regions the pressure decreases as the flow accelerates along the impingement surface. This case is consistent with global continuity considerations. Figure 8a shows the experimental and numerical pressure distributions on the impingement plate in the unconfined jet configuration for different Reynolds number at H/W = 1. Pressure coefficients at the primary stagnation points are greater than one in this spacing. For low spacings, near the stagnation points, the flow rapidly decelerates and therefore the pressure increases significantly. Realizable k-ε model predicts low local pressures for H/W = 1. Hence, significant differences are observed measured and computed data. Discrepancies between calculated and measured results for

H/W = 1 are originated from turbulence model used which is insufficient when the flow is strongly curved. Except for pressure values at the primary subatmospheric regions, there is a better accordance between the measured and computed pressure coefficients on impingement and confinement plates for confined jet configuration at H/W = 1 when comparing with unconfined jet results (Fig. 8b, c). At the H/W = 2, it is shown a good accordance between the experimental and numerical results for unconfined jet while some discrepancies are observed for confined jet especially in the peak pressures at the primary stagnation points of side jet and secondary stagnation points on the impingement plate (Fig. 9a, b). The accordance of measured and predicted local pressure increases as H/W increases

Fig. 11 Effect of the nozzle-to-plate spacing on the computed local Nusselt number distributions for Re = 10,000.
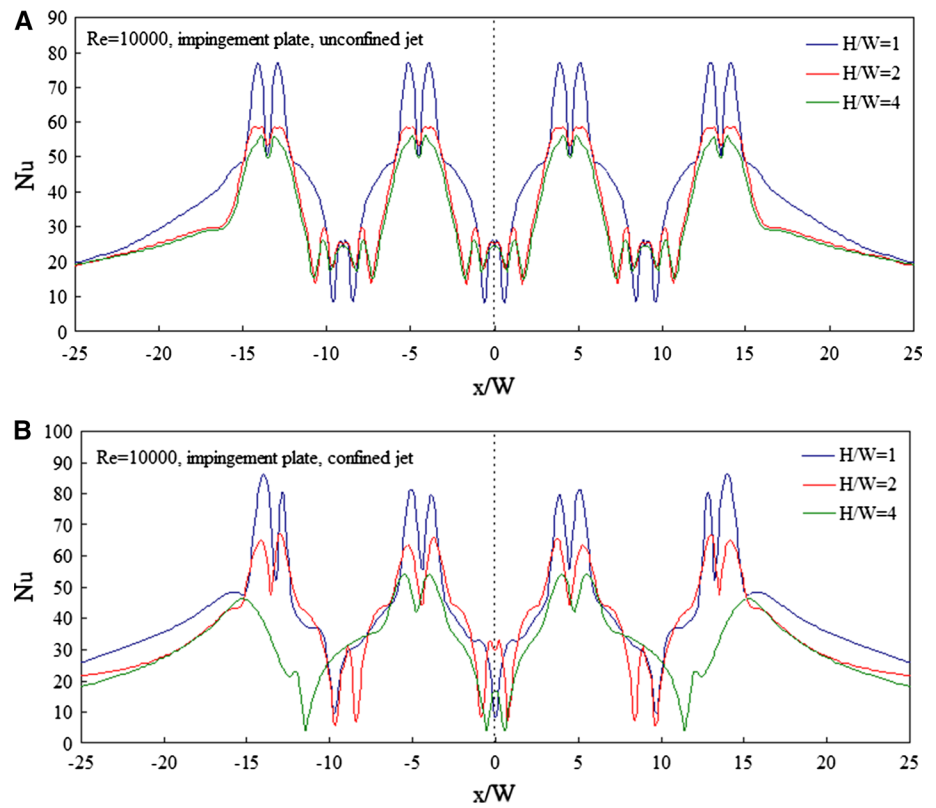**a** Impingement plate in unconfined jet and **b** impingement plate in confined jet

Fig. 12 Effect of the Reynolds number on the computed local Nusselt number distributions for H/W = 2. **a** Impingement plate in unconfined jet and **b** impingement plate in confined jet
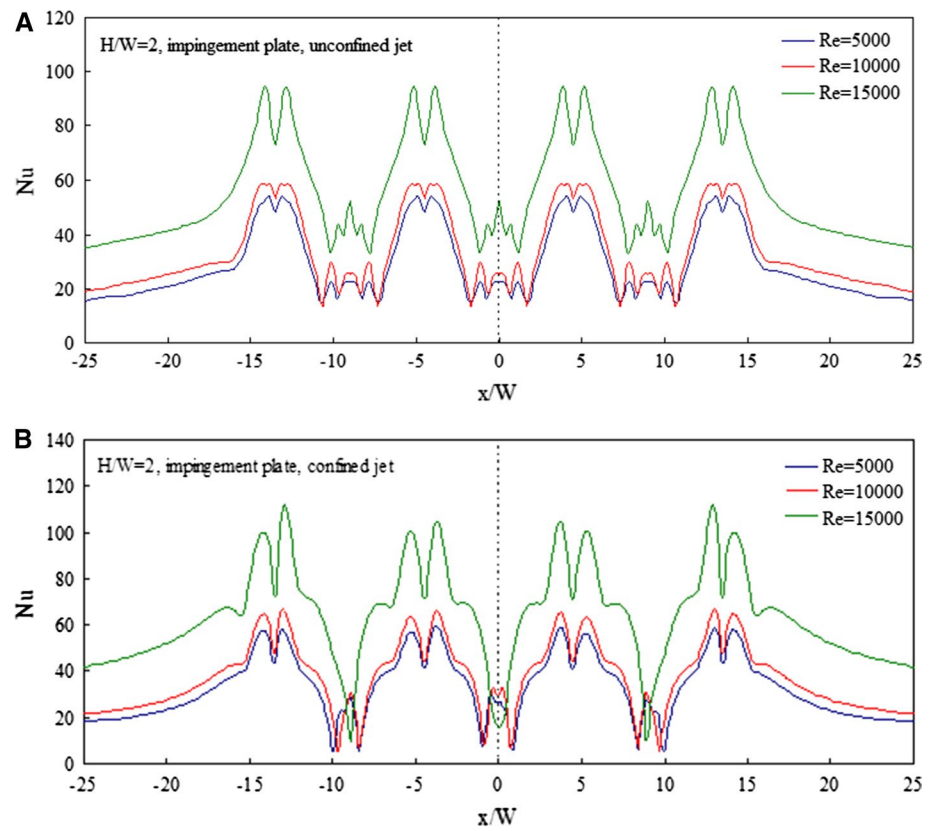
Table 1 Primary stagnation Nusselt numbers obtained numerically

	H/W	Re	Nu$_{stg}$
Unconfined	1	5000	53
Unconfined	1	10,000	76
Unconfined	1	15,000	124
Unconfined	2	5000	52
Unconfined	2	10,000	58
Unconfined	2	15,000	94
Unconfined	3	5000	50
Unconfined	3	10,000	56
Unconfined	3	15,000	88
Unconfined	4	5000	48
Unconfined	4	10,000	54
Unconfined	4	15,000	84
Confined	1	5000	70
Confined	1	10,000	80
Confined	1	15,000	137
Confined	2	5000	57
Confined	2	10,000	66
Confined	2	15,000	111
Confined	3	5000	48
Confined	3	10,000	64
Confined	3	15,000	106
Confined	4	5000	46
Confined	4	10,000	51
Confined	4	15,000	102

(Fig. 10). Although the measured and computed data agree well for large H/W, significant differences between these data are observed for low H/W. Pressure coefficients at the stagnation points are greater than one for H/W < 2, remain constant approximately at one in the range of $2 \leq H/W \leq 4$ and are smaller than one for H/W > 4. It is found that the turbulence model is capable of predicting of the flow and heat transfer characteristics correctly in moderate values of nozzle-to-plate spacings.

4.3 Nusselt distributions

The effect of the nozzle-to-plate spacing (H/W) to the computed Nusselt number distributions on the impingement plate at S/W = 9 and Re = 10,000 are shown in Fig. 11a, b for unconfined and confined jet configurations, respectively. The local Nusselt number was defined as Nu = h W/k_a, where h = q/(T_w − T_j) is convective heat transfer coefficient, T_w and T_j are the impingement wall and jet exit temperatures. It is observed from the figures that the influence of the nozzle-to-plate spacing on the Nusselt number distributions is very significant. A Nusselt number dual peak is observed at around the primary stagnation point

of each jet for both configurations. Dual peak structures observed at the primary stagnation regions is related to the inadequacy of used turbulence model to compute the heat transfer at those regions. Primary stagnation Nusselt numbers and heat transfer ratios increase as the nozzle-to-plate spacing decreases. Small scale peaks are observed at around the secondary stagnation points where neighboring wall jets collide. Nusselt number peaks at the stagnation regions have the same magnitude for the same spacing for unconfined jet case (Fig. 11a). For confined jet configuration, while every four peaks have nearly the same value for H/W = 1 and 2, Nusselt number peaks at around the primary stagnation points of central jets are greater than the Nusselt number peaks of side jets for H/W > 2 spacings (Fig. 11b). Central jets suppress the motion of side jets in the axial direction. Nusselt number takes minimum value at around the secondary stagnation points. Figure 12a, b illustrate the dependence of Nusselt number on Reynolds number at H/W = 2 for unconfined and confined jet configurations, respectively. It is seen from the figures that the local Nusselt number increases with increasing Reynolds number for both configurations. For unconfined jet, four Nusselt number peaks with the same magnitude occur at around the primary stagnation points while small scale peaks occurring at secondary stagnation regions on the impingement plate for all studied Reynolds numbers. For confined jet, beside the Nusselt peaks occured at around the primary stagnation points, at near the both sides of each dual peak, secondary peaks occur in Nusselt distribution. As the secondary peaks become more pronounced with increasing Reynolds number their magnitudes decrease with increasing nozzle-to-plate spacing (Figs. 11b, 12b). Similar findings were also obtained for a single row of circular impinging jets at a large range of Reynolds number [27]. The existence of the secondary peaks in Nusselt number data is mainly explained with the transition from laminar to turbulent flow in wall jet region and increase of the wall-adjacent turbulence level as also mentioned in the study of Attalla and Specht [28]. At the locations of secondary Nusselt peaks, local pressures take negative minimum values in the subatmospheric regions. This situation shows that there exists a linkage between the secondary peak in local Nusselt number and subatmospheric region. When the pressure distributions on the impingement plate for unconfined and confined jet configurations compare each other, it is seen that subatmospheric regions occur only for confined jet case. The comparison of Nusselt distributions on the impingement plate for unconfined and confined jet configurations show that primary stagnation Nusselt numbers and heat transfer ratios is greater in confined jet because of flow confinement and existence of subatmospheric regions. At the secondary stagnation regions, while unconfined jet shows small scale peaks, confined jet presents minimum

values at those regions. Primary stagnation Nusselt numbers numerically obtained on the impingement plate for unconfined and confined jets are represented in Table 1 for different nozzle-to-plate spacings and Reynolds numbers. It is seen that primary stagnation Nusselt numbers increase depending on decreasing nozzle-to-plate spacings and increasing Reynolds numbers.

5 Conclusions

An experimental and numerical investigation was carried out on the flow structure and heat transfer characteristics of unconfined and confined impinging slot jets arrays for Reynolds numbers up to 15,000 at various nozzle-to-plate spacings. As each of jet ejects out of the slot nozzles with parabolic velocity profile, a continuous reduction in velocity occurs while increasing momentum exchange between the jet and the ambient along the axis. Wall jets are formed and spread along impingement plate surface. The wall jets emanating from each impinged form collusions front due to interaction with neighbors. Downwash fountain flows occur between the jets due to the collision of the wall jets and entrainment of ambient air.

Pressure distributions on the surface for both unconfined and confined jet configurations are independent from the Reynolds number and depend on nozzle-to-plate spacing. For unconfined jet, no subatmospheric region is observed on the impingement plate for all the examined Reynolds numbers and spacing. This situation can be explained with the fluid velocity along the impingement plate is lower with respect to the confined jets due to no flow confinement. Local pressures take their maximum values at the primary and secondary stagnation points on the impingement plate. Pressure peaks at primary stagnation points are greater than the peak values at the secondary stagnation points. Peak pressures observed at the point of stagnation of each jet decrease with increasing H/W spacings. For confined jet configuration, three types of subatmospheric regions occur on the impingement and confinement plates depending on H/W and they lie up nearly to the same location on both surfaces. Subatmospheric pressure regions occur on the impingement and confinement plates for H/W up to 8. Subatmospheric regions support the evidence of the recirculation zones occurring on both impingement and confinement surfaces.

Nusselt distributions on the impingement plate for both unconfined and confined jet configurations depend on Reynolds number and nozzle-to-plate spacing. In the unconfined jet, four Nusselt number peaks with the same magnitude occur at around the primary stagnation points while small scale peaks occurring at secondary stagnation regions on the impingement plate. In the confined jet, beside the Nusselt peaks occured at around the primary

stagnation points, at near the both sides of each dual peak, secondary peaks occur in Nusselt distribution. At the locations of secondary Nusselt peaks, local pressures take negative minimum values in the subatmospheric regions. As the Reynolds number is increasing and/or the nozzle-to-plate is decreasing, the Nusslet number peaks become more pronounced. When compared to the results of flow structure and heat transfer, it is seen that there exists a linkage between the subatmospheric regions in pressure distributions and secondary peaks in heat transfer coefficients on the impingement plate. A good qualitative correlation is found among the flow patents, pressure distributions and heat transfer characteristics for various cases investigated. It was found that the effect of confinement on the flow structure and heat transfer is to be very important.

In the numerical part of the study, Realizable k-epsilon turbulence model is used to predict flow filed and heat transfer characteristics. From the comparisons of numerical results with experimental ones, it is found that the model is capable of predicting the flow and heat transfer characteristics correctly in moderate values of nozzle-to-plate spacing.

References

1. Martin H (1997) Heat and mass transfer between impinging gas jets and solid surfaces. Adv Heat Transf 13:1–60
2. Polat S, Huang B, Mujumdar AS, Douglas WJM (1989) Numerical flow and heat transfer under impinging jets: a review. Ann Rev Numer Fluid Mech Heat Transf 2:157–197
3. Bernhard W, Sebastian S (2009) Multiple jet impingement: a review. International Symposium on Heat Transfer in Gas Turbine Systems, Antalya, pp 23–40
4. Huber AM, Viskanta R (1994) Effect of jet–jet spacing on convective heat transfer to confined impinging arrays of axisymmetric air jets. Int J Heat Mass Transf 37:2859–2869
5. Saad NR, Polat S, Douglas WJM (1992) Confined multiple impinging slot jets without cross flow effects. Int Heat Fluid Flow 13:2–14
6. Yang Y, Shyu C (1998) Numerical study of multiple impinging slot jets with an inclined confinement surfaces. Numer Heat Transf Part A 33:23–37
7. Koopman RN (1975) Local and average transfer coefficients for multiple impinging jets. PhD thesis, University of Minesota
8. Kwok LC, Leung CW, Cheung CS (2005) Heat transfer characteristics of an array of impinging pre-mixed slot flame jets. Int J Heat Mass Transf 48:1727–1738
9. Ozmen Y (2011) Confined impinging twin air jets at high Reynolds numbers. Exp Therm Fluid Sci 35:355–363
10. Koopman RN, Sparrow EM (1976) Local and average transfer coefficients due to an impinging row of jets. Int J Heat Mass Transf 19:673–683
11. Chander S, Ray A (2007) Heat transfer characteristics of three interacting methane/air flame jets impinging on a flat surface. Int J Heat Mass Transf 50:640–653
12. Pan Y, Webb BW (1995) Heat transfer characteristics of arrays of free-surface liquid jets. J Heat Transf 117(4):878–883
13. San JY, Tsou YM, Chen ZC (2007) Impingement heat transfer of staggered arrays of air jets confined in a channel. Int J Heat Mass Transf 50:3718–3727

14. Rady M, Arquis E (2006) Heat transfer enhancement of multiple impinging slot jets with symmetric exhaust ports and confinement surface protrusions. Appl Therm Eng 26:1310–1319

15. Prasad KD, Kumar KR, Sastry MRCH (2012) Fluid flow and heat transfer analysis of turbulent multiple circular jets impinging on a flat plate. Int J Eng Res Appl 2(5):1976–1985

16. Fernandez JA, Elicer-Cortes JC, Valencia A, Pavagean M, Gupta S (2007) Comparison of low cost two equation turbulence models for prediction flow dynamics in twin jet devices. Int Commun Heat Mass Transf 34:570–578

17. Aldabbagh LBY, Sezai I (2002) Numerical simulation of three-dimensional laminar, square twin-jet impingement on a flat plate, flow structure and heat transfer. Numer Heat Transf Part A 41:835–850

18. Chuang SH, Chen MH, Lii SW, Tai FM (1992) Numerical simulation of twin-jet impingement on a flat plate coupled with cross-flow. Int J Numer Methods Fluids 14:459–475

19. Chuang SH, Nieh TJ (2000) Numerical simulation and analysis of three dimensional turbulent impinging square twin jet flow field with no-cross flow. Int J Numer Methods Fluids 33:475–498

20. Seyedein SH, Hasan M, Mujumdar AS (1995) Turbulent flow and heat transfer from confined multiple impinging slot jets. Numer Heat Transf 18:35–51

21. Xing Y, Spring S, Weigand B (2010) Experimental and numerical investigation of heat transfer characteristics of inline and staggered arrays of impinging jets. J Heat Transf 132:1–11

22. Kumar MA, Prasad BVSSS (2011) Computational flow and heat transfer of multiple circular jets impinging on a flat surface with effusion. Heat Mass Transf 47:1121–1132

23. Mikhail S, Morcos SM, Abou-Ellail MMM, Ghaly WS (1982) Numerical prediction of flow field and heat transfer from a row of laminar slot jets impinging on a flat plate. Heat Transf 3:377–382

24. Cziesla T, Tandogan E, Mitra NK (1997) Large-eddy simulation of heat transfer from impinging slot jets. Numer Heat Transf Part A 32:1–17

25. Coussirat M, van Beeck J, Mestres M, Egusquiza E, Buchlin JM, Valero C (2005) Computational fluid dynamics modeling of impinging gas-jet systems. Trans ASME 127:704–713

26. Garimella SV, Schroeder VP (2001) Local heat transfer distributions in confined multiple air jet impingement. ASME J Electron Packag 123(3):165–172

27. Kumar MA, Prasad BVSSS (2009) Computational investigations of flow and heat transfer on an effused concave surface with a single row of impinging jets for different exit configurations. Eng Appl Comput Fluid Mech 3(4):530–542

28. Attalla M, Specht E (2009) Heat transfer characteristics from in-line arrays of free impinging jets. Heat Mass Transf 45:537–543